Chapter IV. Site-directed electrodeposition of biorecognition nanomodules as biochip arraying technique

Abstract

The goal of the present work is to selectively electrodeposit oligonucleotide-modified colloidal gold conjugates (biorecognition nanomodules) with photolithographic resolution to yield a new arraying method for the production of high-density multi-addressable biosensing chips.

It is shown by light and electron microscopy that selective electrodeposition of colloidal gold on 5µm interdigitated electrodes (IDEs) can be achieved. Selective electrodeposition on indium-tin oxide (ITO) electrodes was proven by spectrophotometry. In all the cases, colloidal gold could be selectively deposited in short times (from 1 to 5min) applying from +0.8 to +1.2V (*vs.* Ag/AgCl). Piezoelectric techniques also demonstrated the selective electrodeposition of colloidal gold.

Oligonucleotide-colloidal gold biorecognition nanomodules were then electrodeposited on several electrode surfaces. Light microscopy proved the selective electrodeposition on IDEs and 3-electrode arrays, the optimal conditions being +0.8V (*vs.* Ag/AgCl) for 10min. Electrochemical techniques proved the selective deposition on glassy carbon electrodes in 2min with +1.1V (*vs.* Ag/AgCl) applied potential. The conjugates were also electrodeposited on carbon screen-printed electrodes applying +1.2V (*vs.* Ag/AgCl) for 2min, and the immobilisation was proved by colourimetric and electrochemical methods, showing a non-specific adsorption of 14%.

Electrodeposited nanomodules were functional after their electrodeposition, and able to differentiate 4-point mutations in 19-mer oligonucleotide sequences, demonstrating that this arraying strategy can be used in low cost DNA sensor arrays.

Keywords: colloidal gold, biorecognition nanomodules, HRP-colloidal gold conjugate, oligonucleotide-colloidal gold conjugate, DNA chip array, mutation detection.

Introduction

There is little doubt that low cost biosensors can change the way in which analytical procedures are performed in clinical diagnosis, environmental and food analysis. Key to the utility and low cost of these analytical devices is the ability to make multi-analyte sensors. Miniaturisation and integration are therefore the most urgent requirements for biosensors and biochips, in order to minimise sample volumes, invasiveness, reagent and other general costs, and to obtain ready-to-use portable devices.

One of the key parameters in the DNA chip design is the immobilisation step. Not only it is necessary to retain the functionality of the biomolecule after the immobilisation, but also to achieve

a high attachment efficiency and density. Site-specific immobilisation at high density has been attempted for several years. Specific arraying methods, like ink-jetting (Castellino *et al.*, 1997), pin deposition (Yershov *et al.*, 1996; Drobyshev *et al.*, 1997; and Guschin *et al.*, 1997; Sakai *et al.*, 2000; and Zammatteo *et al.*, 2000), polypyrrolisation (Livache *et al.*, 1994, 1995 and 1998; and Roget *et al.*, 1995) and photolithography (Fodor *et al.*, 1991; and Pease *et al.*, 1994), provide ordered arrangement of different oligonucleotides fixed to specific positions on a solid surface with varying resolution. However, each one of the techniques presents relative disadvantages. The main problem of ink-jetting is the ease and robustness of the method. Air bubbles or clogging reduce the repeatability and reliability of the system, and lead to maintenance problems. Poor uniformity of the deposit may result, which can cause crossover contamination between probes. In the pin deposition technique, excessive splashing is also a problem leading to variability in spot size and in probe concentration. Polypyrrolisation presents the drawbacks of wet chemistry, which increases the irreproducibility of the system, and the necessity of a washing step after each polypyrrole synthesis to avoid cross-contamination with residual oligonucleotides. In photolithography, the main drawback is the inability to control the sequence quality, and the fact that possible mistakes in the synthesis make necessary a high number of redundant sites. This work is focused on the development of a new immobilisation and arraying method, based on the site-directed electrodeposition of biorecognition modules. These biorecognition modules are formed by the conjugation of the biorecognition element or functional biomolecule to a colloidal gold particle that acts as immobilisation vehicle. Despić and Pavlović (1984) took benefit of the electrophoretic mobility of colloidal gold to deposit it at a carbon electrode. Apart from bare colloidal gold, several scientists used colloidal gold to immobilise enzymes on their sensors by electrodeposition. For example, Crumbliss *et al.* (1992) conjugated glucose oxidase (GOx), horseradish peroxidase (HRP) and xanthine oxidase to colloidal gold and electrodeposited these conjugates onto platinum or glassy carbon by applying +1.6V (*vs.* Ag/AgCl) for 2h. These enzyme electrodes gave an electrochemical response to the corresponding enzyme substrates in the presence of ferrocene mediators, demonstrating the utility of colloidal gold as biocompatible matrix suitable for the fabrication of enzyme electrodes. Following the same strategy, our work is focused to the selective electrodeposition of bio/nanoconjugates of colloidal gold with oligonucleotides. The nanomodular approach presented in this paper can be used to build DNA sensor microarrays with high resolution (only limited by the electrode pattern, i.e. with photolithographic resolution) and the possibility to previously control the quality of the probes. Arraying with these characteristics is achieved with low cost equipment once the photolithographed substrate is available. Furthermore, the technique is compatible with well-developed processes in the semiconductor industry. With both arraying and measurement by electrochemical methods, overall fabrication costs can be lower. Moreover, the versatility of the strategy makes it a generic approach, useful for any kind of sensing chip, where high resolution might be needed, be it enzymatic, affinity or chemical. Of importance in this technique is the avoidance of non-specific adsorption.

Relating to this, it is considered to briefly examine what is known about deposition of colloidal suspensions on solid surfaces. Colloidal gold particles have a negatively charged surface, property that can be used to deposit them on surfaces under applied electric fields (Despić and Pavlović, 1984; Giersig and Mulvaney, 1993; and Bailey *et al.*, 2000). When like-charged colloidal particles are immobilised on a surface of opposite charge, the interparticle repulsion decreases due to electrohydrodynamic and electroosmic effects, favouring the ordered and close packing (Giersig and Mulvaney, 1993), unlike simply adsorbed colloidal particles on neutral surfaces (Grabar *et al.*, 1996). In fact, although several particle adsorption models, e.g. Random Sequential Adsorption (RSA), describe an irreversible particle adsorption (Adamczyk *et al.*, 1994 and 1997, and Adamczyk and Weroński, 1997), the aforementioned electrohydrodynamic and electroosmic effects might favour the mobility of the adsorbed particle. In fact, these models are being refined to consider not only these effects, but also transport mechanisms, such as diffusion and convection (Lavalle *et al.*, 1999; Wojtaszczyk *et al.*, 1997; and Faraudo and Bafaluy, 1999).

In this work, the electrodeposition of colloidal gold and biorecognition nanomodules on different electrode surfaces and the detection of selective deposition by a variety of methods are described. Firstly, bare colloidal gold was electrodeposited on photolithographed gold interdigitated electrodes (IDEs), indium-tin oxide (ITO) and gold-covered quartz crystals, and the selective electrodeposition was detected by microscopic, spectrophotometric and piezoelectric methods, respectively. Secondly, HRP-colloidal gold conjugate was deposited on screen-printed electrodes and the deposition was characterised by colourimetry. Finally, selective depositions of oligonucleotide biorecognition nanomodules on photolithographed gold IDEs and photolithographed gold 3-electrode arrays were shown by microscopy, depositions on glassy carbon were shown by electrochemistry, and depositions on carbon screen-printed electrodes were shown by colourimetry and electrochemistry. For each one of the electrodepositions, the operational parameters were optimised in order to use minimum potential and short deposition times. Hybridisation of electrodeposited oligonucleotide-colloidal gold conjugates with complementary sequences and sequences with 4-point mutations was followed by electrochemistry, demonstrating the functionality of the bio/nanomodules after their immobilisation.

Materials and methods

Materials. 5nm (4.9 $\pm$ 0.7nm) and 20nm (21.7 $\pm$ 2.0nm) diameter colloidal gold, and HRP-10nm colloidal gold conjugate (9.3 $\pm$ 0.5nm) were obtained from Sigma. The original concentrations were 4.4 x 10^{13}, 4.9 x 10^{11} and 3.2 x 10^{13} particles mL^{-1} for 5, 20nm colloidal gold and HRP-10nm colloidal gold, respectively. Unconjugated gold colloids contained about 0.01% $HAuCl_4$ suspended in 0.01% tannic acid with 0.04% trisodium citrate, 0.26mM potassium carbonate and 0.02% sodium azide as preservative. HRP-colloidal gold was a suspension in 50% glycerol with 0.15M NaCl, 0.01M MES, pH 6.5, 0.25% BSA (no sodium azide was added because it inhibits the peroxidase

activity). 3nm (3 ± 1nm) diameter colloidal gold was a gift from Dr. Ewen Smith (University of Strathclyde, Glasgow, United Kingdom). Polyoxyethylenesorbitan monolaurate (Tween 20), bovine serum albumin (BSA), streptavidin-HRP and 3,3',5,5'-tetramethyl-benzidine liquid substrate system for ELISA (TMB) (containing TMB and H_2O_2 in an slightly acidic buffer) were also purchased from Sigma. Antidigoxigenin-HRP Fab fragments (antidig-HRP) were obtained from Roche. FITC-oligonucleotide-thiol-colloidal gold conjugate, the oligonucleotide being 3' FITC-$(C)_{12}(T)_{20}(C)_{12}$-SH 5', and digoxigenin(dig)-oligonucleotide-thiol-colloidal gold conjugate, the oligonucleotide being 3' digoxigenin-ACTTAACCGAGTCGACCGA-SH 5', were obtained by conjugation of 3 or 20nm colloidal gold with oligonucleotides from Genosys and Eurogentec, respectively. 3' TCGGTCGACTCGGTTAAGT 5' (complementary), 3' TCGGTCGACTCGGTTAAGT-biotin 5' (biotin-labelled complementary) and 3' TCGGTGGGCTCG GGTGAGT-biotin 5' (biotin-labelled with 4-point mutations) were from Eurogentec. Indium-tin oxide (ITO) surfaces were purchased from Delta Technologies, Ltd. 5μm interdigitated gold electrodes (IDEs) were from ABTECH Scientific Inc. 1.5mm diameter glassy carbon electrodes were from Cypress Systems. 5MHz gold-covered quartz crystals were purchased from Maxtek, Inc. Photolithographed 1mm diameter gold 3-electrode arrays were in-house designed and fabricated by NMRC (National Microelectronics Research Centre) of Ireland.

Instrumentation. Electrodepositions and chronoamperometries were performed using an AUTOLAB PGSTAT10 potentiostat in a conventional three-electrode cell, with Ag/AgCl as reference electrode and Pt as counter electrode or in a two-electrode system (for the screen-printed electrodes), with screen-printed Ag/AgCl as reference and counter electrode. Absorbance values and full spectra were measured with an HP 8453 spectrophotometer or with a Molecular Devices 340PC 96-well plate reader. Fluorescence was measured with a Perkin Elmer LS-50 fluorimeter or with a Nikon E600FN fluorescence microscope equipped with a Sony CCD camera. The fluorescence microscope in the transmittance mode was used for light microscopy. Electron microscopy was performed with a Zeiss 10 Ca electron microscope. All solutions were made from distilled water purified through a Milli-Q water system. Frequency measurements were performed with a PM-710 Electrochemical Quartz Crystal Microbalance plating monitor from Maxtek, Inc. The flow-cell used in the removal of non-specifically adsorbed particles from photolithographed gold surfaces was a loan of Trace Biotech AG.

Site-directed colloidal gold electrodeposition on photolithographed gold IDEs, ITO electrodes and gold-covered quartz crystals. For the electrodeposition of 5nm colloidal gold on photolithographed gold IDEs, firstly the IDEs were cleaned with "piranha's solution" (70% H_2SO_4 : 30% H_2O_2) and cyclic voltammetry (10 scans between -0.3 and +1.7V (*vs.* Ag/AgCl) at 0.5V s^{-1} in 0.33M H_2SO_4). Afterwards, the IDEs were immersed in a three-electrode cell containing 5nm colloidal gold suspension (4.4×10^{11}, 2.2×10^{12} and 4.4×10^{12} particles mL^{-1} in 10mM phosphate buffer, 0.1M NaCl, pH 7.0), and from +1.0 to +1.6V (*vs.* Ag/AgCl) was applied at one of the two sets

for 10, 20 and 30min. The set at which no potential was applied was used as control to measure non-specific adsorption. The deposition was characterised by light microscopy, electron microscopy and electrochemistry. For the electrochemical detection, linear sweep voltammetry (LSV) was performed between -0.3 and +1.7V (*vs.* Ag/AgCl) at 0.05mV s^{-1} in 0.1M H_2SO_4.

Transparent ITO electrodes were cleaned as follows: sonication in Alconox for 15min, sonication in 2-propanol for 15min and sonication in water for 15min twice. Two different detection modes were set up. *Sampling:* the electrodeposition (+0.8 and +1.6V (*vs.* Ag/AgCl) for 1, 2, 5, 10, 20, 25 and 30min) was performed in a three-electrode conventional cell containing 5 or 20nm colloidal gold suspension (4.4 x 10^{13} and 5.2 x 10^{11} particles mL^{-1}, respectively, in 10mM phosphate buffer, 0.1M NaCl, pH 7.0) and the ITO electrode was then immersed in a spectrophotometric cuvette filled with water or with colloidal gold suspension for absorbance measurement. *Real-time monitoring:* the electrodeposition (+0.8V (*vs.* Ag/AgCl) for 30min) was carried out at the same time as the detection, the counter and the reference electrode being included in a three-electrode spectrophotoelectrochemical thin cuvette / cell (200µL of volume, 0.05cm light path) containing 5nm colloidal gold suspension (4.4 x 10^{13} particles in 10mM phosphate buffer, 0.1M NaCl, pH 7.0). No potential was applied at the controls.

Colloidal gold was also electrodeposited on 5MHz gold-covered quartz crystals in an in-house made electrochemical flow-cell at a rate of 75µL min^{-1}. Firstly, 10mM tris-HCl buffer, 10mM KCl, 1% BSA, pH 7.0, was circulated trough the cell and the frequency was monitored. Once the frequency stabilised, +1.2V (*vs.* Ag/AgCl) was applied to the gold-covered quartz crystal. Once the frequency stabilised again, the solution was changed by a colloidal gold suspension (4.2 x 10^{11} particles in the same buffer). 10min after the colloidal gold injection, the potential was stopped.

Removal of non-specifically adsorbed colloidal gold particles. Some preliminary experiments were performed in a flow system to study the effect of the Reynolds number on the removal of non-specifically adsorbed colloidal gold on photolithographed gold electrodes. After deposition of a 50-µL drop of the colloidal gold suspension (8.5 x 10^{11} particles mL^{-1} in 10mM tris-HCl buffer, 10mM KCl, 1% BSA, pH 7.0) on the electrode and application of +1.6V (*vs.* Ag/AgCl) for 10min (no potential was applied to the blanks), the arrays were introduced into the flow-cell and the same buffer without colloidal gold was circulated firstly for 10min at 0.07mL min^{-1}, and afterwards for 10min at 6.20mL min^{-1}. Electrodes were observed under light microscopy before and after each experiment. Phase analysis was performed with the microscope AnalySIS software.

HRP-bionanomodule arraying. A 2-µL drop of HRP-colloidal gold conjugate suspension (3.2 x 10^{13} particles mL^{-1} in 50% glycerol with 0.15M NaCl, 0.01% MES, pH 6.5, 0.25% BSA) was deposited on screen-printed electrodes and +0.8V (*vs.* Ag/AgCl) was applied for 1 and 5min. No potential was applied at the control electrodes. After rinsing, the electrodes were incubated in

commercial TMB liquid substrate for 1h at 37°C with stirring, and the reaction was stopped with H_2SO_4. The colourimetric response was monitored at the 96-well plate reader.

Biorecognition nanomodule electrodeposition. The FITC-oligonucleotide-thiol-colloidal gold conjugate (1.8 x 10^{12} particles mL^{-1} in 10mM phosphate buffer, 0.1M NaCl, pH 7.0) was deposited on one of the sets of the IDEs (+1.6V (*vs.* Ag/AgCl) for 2h) and the deposition was characterised by light microscopy. The set at which no potential was applied was used as control.

The FITC-oligonucleotide-thiol-colloidal gold conjugate (7.7 x 10^{11} particles mL^{-1} in 10mM phosphate buffer, 0.1M NaCl, pH 7.0) was also electrodeposited on glassy carbon electrodes by applying +1.1V (*vs.* Ag/AgCl) for 2min, +0.8V (*vs.* Ag/AgCl) for 5min, and +0.6V (*vs.* Ag/AgCl) for 10min. No potential was applied at the controls. None of the microscopy characterisation techniques could be used and the electrodeposition was detected by cyclic voltammetry (CV) at 0.05V s^{-1} in 0.1M H_2SO_4.

The dig-oligonucleotide-thiol-colloidal gold conjugate was firstly used in sandwich ELONA on screen-printed electrodes (Scheme IV.1).

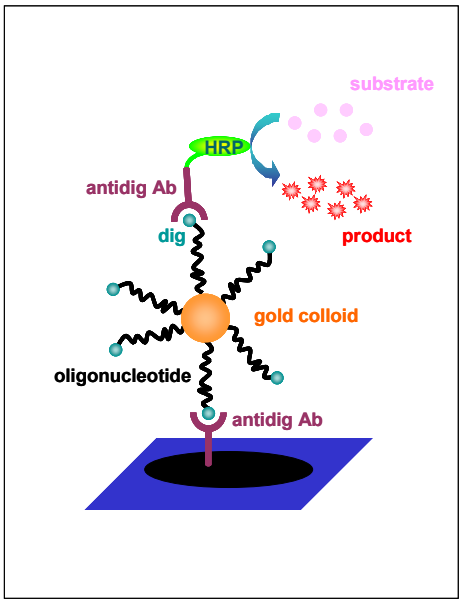

Scheme IV.1. Sandwich ELONA with dig-oligonucleotide-thiol-colloidal gold (20nm) on a carbon screen-printed electrode. The electrode is coated by antidigoxigenin; the digoxigenin of the dig-oligonucleotide-thiol-colloidal gold conjugate recognises the antidigoxigenin; the antidig-HRP recognises the digoxigenin of the immobilised dig-oligonucleotide-thiol-colloidal gold conjugate; the HRP label reacts with its substrate to give a coloured product.

The dig-oligonucleotide-thiol-colloidal gold conjugate was electrochemically deposited on screen-printed electrodes (Scheme IV.2). The electrodes were firstly blocked with BSA. After rinsing, a 0.5-µL drop of dig-oligonucleotide-thiol-colloidal gold conjugate (1.3 x 10^{12} particles mL^{-1} in 0.1M tris-HCl buffer, 0.1M KCl, pH 8.0, 1% BSA) was placed on the screen-printed electrode and +1.2V (*vs.* Ag/AgCl) was applied for 2min. No potential was applied at the controls. FITC-oligonucleotide-thiol-

colloidal gold conjugate (1.2 x 10^{12} particles mL^{-1} in 0.1M tris-HCl buffer, 0.1M KCl, pH 8.0, 1% BSA) was also used as control. The electrodes were then rinsed and incubated in antidig-HRP. For the colourimetric detection, dig-oligonucleotide-thiol-colloidal gold conjugate was used, and the electrodes were incubated in commercial TMB liquid substrate and absorbance values were measured at 650nm. For the electrochemical detection, dig-oligonucleotide-thiol-colloidal gold conjugate was used, and 1µL of H_2O_2 (1:500 dilution in 50mM acetate buffer, 0.15M NaCl, pH 5.1) and 1µL of [Os(2,2'-bipyridine)$_2$Cl(4-(aminomethyl)pyridine)]Cl (0.2mM in water) were mixed and placed on the working electrode. After 2-min incubation, -0.1V (*vs.* Ag/AgCl) was applied for 1min and the current values at different times were measured (control and blank electrodes were examined as stated).

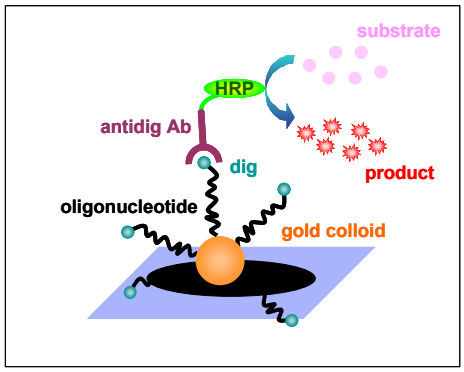

Scheme IV.2. Electrodeposited dig-oligonucleotide-thiol-colloidal gold (20nm) on a carbon screen-printed electrode. The dig-oligonucleotide-thiol-colloidal gold conjugate is electrodeposited on the carbon screen-printed electrode; the antidig-HRP recognises the digoxigenin of the electrodeposited dig-oligonucleotide-thiol-colloidal gold conjugate; the HRP label reacts with its substrate to give a coloured product.

The dig-oligonucleotide-thiol-colloidal gold conjugate was also electrochemically deposited on photolithographed gold 3-electrode arrays. A 15-µL drop of dig-oligonucleotide-thiol-3nm colloidal gold conjugate (1.3 x 10^{12} particles mL^{-1} in 0.05M tris-HCl buffer, 0.05M KCl, pH 8.0, 1% BSA) was placed on two gold electrodes of the 3-electrode array and from +0.8 to +1.9V (*vs.* Ag/AgCl) was applied for 1-10min to one of them. No potential was applied at the other gold electrode. The third gold electrode was used as blank (no potential, no colloidal gold conjugate). The array was then rinsed and observed under light microscopy, and the brightness was evaluated with the phase analysis of the microscope AnalySIS software.

Functionality of electroarrayed biorecognition nanomodules. The dig-oligonucleotide-thiol-colloidal gold conjugate was used in a hybridisation ELONA on carbon screen-printed electrodes (Scheme IV.3, but measuring the colourimetric response instead of the electrochemical one). For the hybridisation step, after the colloidal gold incubation like in the previous section, the electrodes were introduced in 70µL of a solution of biotin-labelled complementary oligonucleotide, non-labelled complementary oligonucleotide or biotin-labelled oligonucleotide with 4-point mutations (5µg mL^{-1} in 10mM tris-HCl, 1mM EDTA, 0.3 x SSC, 2 x Denhardt's solution, pH 8.0, corresponding to 4.7 x 10^{14} oligonucleotide molecules per mL) for 1h at 55°C with stirring, and rinsed with water and with

0.1mM tris-HCl buffer, 0.1% Tween 20. The electrodes were then incubated in 50μL of a streptavidin-HRP solution (0.4μg mL^{-1} in 0.1M tris-HCl buffer, 0.1M KCl, pH 8.0, 1% BSA) for 1h at 37°C with stirring, and rinsed with water and with 0.1mM tris-HCl buffer, 0.1% Tween 20. Finally, the electrodes were incubated in 50μL of commercial TMB liquid substrate for 1h at 37°C with stirring protected from light and absorbance values were measured at 650nm. Appropriate blanks and control experiments were performed as mentioned.

The dig-oligonucleotide-thiol-colloidal gold conjugate was electrochemically deposited on carbon screen-printed electrodes like in the previous section and hybridisation was detected electrochemically (Scheme IV.3). No potential was applied at the controls. In the hybridisation step, biotin-labelled complementary sequences and oligonucleotides with 4-point mutations were used. After incubation in streptavidin-HRP, hybridisation from electrodeposited conjugates was detected electrochemically following the same detection system as for the antidig-HRP label.

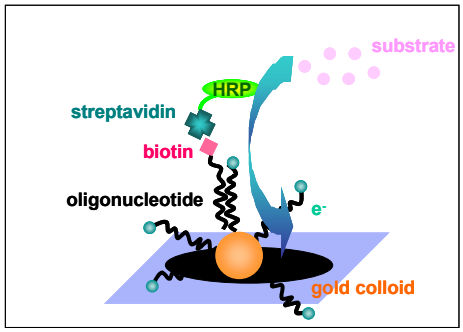

Scheme IV.3. Electrodeposited dig-oligonucleotide-thiol-colloidal gold (20nm) on a carbon screen-printed electrode and subsequent hybridisation. The dig-oligonucleotide-thiol-colloidal gold conjugate is electrodeposited on the carbon screen-printed electrode; the oligonucleotide of the dig-oligonucleotide-thiol-colloidal gold conjugate hybridises with its complementary sequence; the streptavidin-HRP recognises the biotin of the complementary oligonucleotide; the HRP label reacts with its substrate to give an electrochemical signal.

Results and discussion

Site-directed colloidal gold electrodeposition on photolithographed gold IDEs, ITO electrodes and gold-covered quartz crystals. Firstly, microarraying with photolithographic resolution using unmodified colloidal gold has been attempted. Light and electron microscopy demonstrated the site-directed deposition of the colloidal gold on interdigitated electrodes (5-μm width gap and lines). Figure IV.1 shows a portion of the gold IDEs before and after immersion in a colloidal gold suspension (4.4 x 10^{12} particles in 10mM phosphate buffer, 0.1M NaCl, pH 7.0) and application of +1.0V (*vs.* Ag/AgCl) for 30min at one of the sets. Lower concentrations and times did not provide detectable electrodeposition with light microscopy, and higher applied potentials provoked colloidal gold aggregation. The pink lines correspond to the electrodes and the blue lines to the gap between them. It can be clearly seen that whilst the lines corresponding to the set at which no potential has been applied remain at the same colour (small differences due to the imaging set up), the lines associated to the set at which +1.0V (*vs.* Ag/AgCl) has been applied for

30min show a different colour (orange). This observation demonstrates the selective electrodeposition of 5nm colloidal gold on 5μm electrodes.

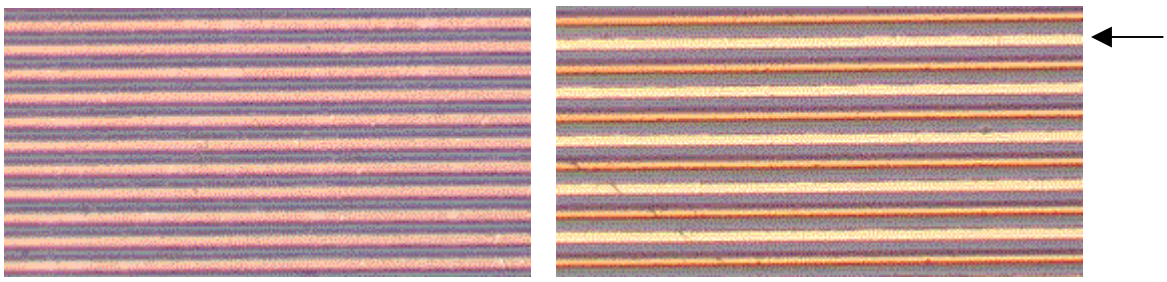

a) b)

Figure IV.1. Gold IDEs (5-μm width electrodes and gap) under light microscopy a) before and b) after immersion in a 5nm colloidal gold suspension in a three-electrode cell and application of +1.0V (*vs.* Ag/AgCl) for 30min at one of the sets. No potential was applied at the control set. Arrow indicates control set.

Under these conditions, a thick multilayer of colloidal gold has been formed. Surface hydrodynamic stresses of this structure led to detachment of the electrodeposited material as if it were a new dense phase (Figure IV.2). This observation settles to some extent the controversy on the reversibility of the deposition phenomenon. Since for the application of DNA sensors a multilayer structure is not necessary, in subsequent experiments it has been tried to limit the extent of electrodeposition by lowering the exposure time in the hope that the non-specific adsorption phenomena would also be limited.

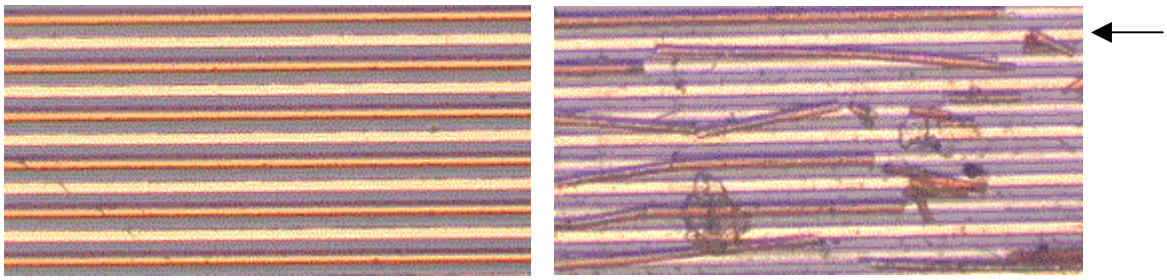

a) b)

Figure IV.2. Gold IDEs (5-μm width electrodes and gap) under light microscopy after immersion in a 5nm colloidal gold suspension in a three-electrode cell, application of +1.0V (*vs.* Ag/AgCl) for 30min at one of the sets and a) carefully rinsing or b) water-jet rinsing. No potential was applied at the control set. Arrow indicates control set.

Electron microscopy was also used to characterise the site-directed electrodeposition of colloidal gold on gold IDEs. Figure IV.3 shows a portion of the IDEs after electrodeposition under the same conditions. The white lines correspond to the electrodes and the black lines to the gaps between them. The electrode lines at which the potential has been applied present a rougher surface, with an irregular silhouette representing electrodeposited colloidal gold particles. This site-directed electrodeposition was also detected with electrochemistry. At the electrode where potential was applied, it was possible to see an oxidation peak at approximately +1.2V (*vs.* Ag/AgCl) that

corresponds to the electrodeposited colloidal gold oxides formation (Figure IV.4). The intensity of this peak is substantially higher than the intensity of the peak corresponding to the electrode where no potential was applied. This increase in intensity corresponds most likely to the surface area increase and the higher catalytic efficiency of the nanostructured material. Additionally, the peak intensity corresponding to the passive adsorption does not differ from the peak intensity of the background caused by the gold IDEs (*result not shown*). Another oxidation peak at approximately +1.5V (*vs.* Ag/AgCl) appears in the linear sweep voltammetry on the electrode where potential was applied. This peak could correspond to another gold oxidation mechanism that appears when there is electrodeposited material on the electrode. These site-directed electrodeposition experiments on IDEs have demonstrated that the strategy is suitable for arraying colloidal gold with photolithographic resolution.

Figure IV.3. Gold IDEs (5-µm width electrodes and gap) under electron microscopy after immersion in a 5nm colloidal gold suspension in a three-electrode cell and application of +1.0V (*vs.* Ag/AgCl) for 30min at one of the sets. No potential was applied at the control set. Arrow indicates control set.

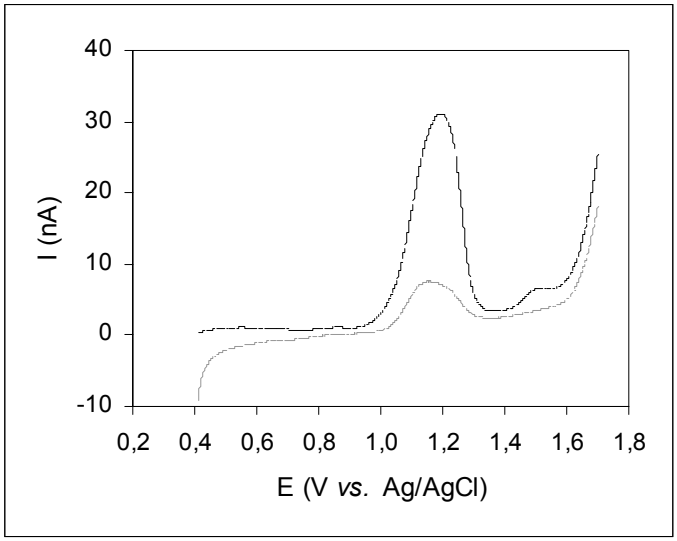

Figure IV.4. Linear sweep voltammetry at 0.05mV s^{-1} in 0.1M H_2SO_4 after selective electrodeposition of 20nm colloidal gold by immersion of the gold IDEs in a three-electrode cell and application of +1.0V (*vs.* Ag/AgCl) for 30min at one set (dark blue). No potential was applied at the control set (light blue).

Colloidal gold deposition on transparent ITO electrodes was characterised by *sampling* and *real-time monitoring* spectrophotometric techniques (*see experimental section*). The *sampling* mode showed absorbance peaks at 523nm only when potential had been applied (Figure IV.5). This peak corresponds to the electrodeposited colloidal gold particles on the ITO, since the colloidal gold suspension absorbs at this wavelength. Although after 1min differences between electrodeposition and passive adsorption were not observed (no absorbance peaks at 523nm in any of the spectra, *results not shown*), after 2min the differences were noticeable and at higher times more evident. The highest differences between electrodeposited and non-specifically adsorbed colloids were achieved at longer times. However, since at short times the absorbance of non-specifically adsorbed particles is negligible, it seems that they are advantageous for arraying. However, the detection limit of this method should be taken into consideration when making this assertion. The short-time regime is interesting from two points of view. Firstly, it is very probable that the kinetics of non-specific adsorption and of electrodeposition are different. It is expected that during electrodeposition, a plateau coverage can be reached in short times, whilst the non-specific adsorption is slower. Secondly, if electrodeposition can be done at 1-min range, arraying can be fast enough to compete with pin deposition or ink-jetting. Higher electrodeposition potentials (+1.6V (*vs.* Ag/AgCl)) resulted in aggregation of the colloidal gold suspension in the spectroelectrochemical cell the colour of the solution changing from pink to blue.

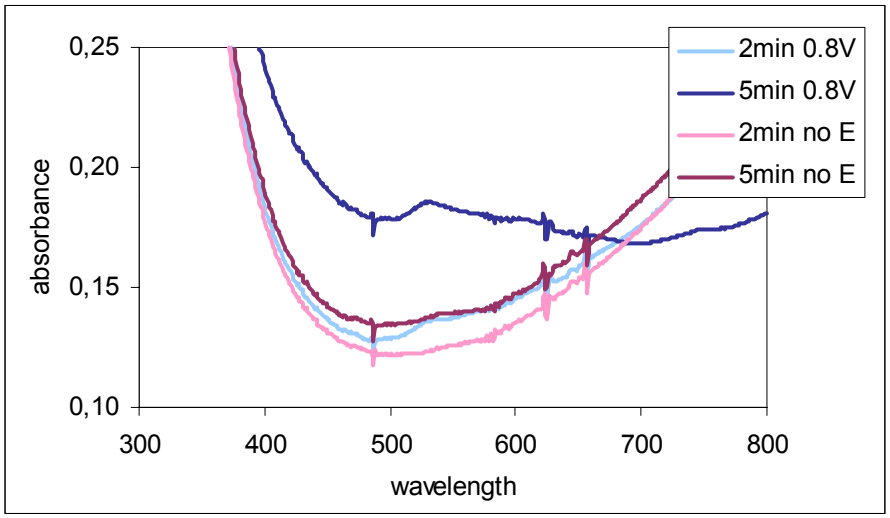

Figure IV.5. Absorbance *vs.* wavelength of 20nm colloidal gold electrodeposited or adsorbed on ITO electrodes in *sampling* mode. Electrodeposition conditions: application of +0.8V (*vs.* Ag/AgCl) for 2 and 5min to a working ITO electrode immersed in a three-electrode cell containing 20nm colloidal gold suspension (5.2 x 10^{11} particles mL^{-1} in 10mM phosphate buffer, 0.1M NaCl, pH 7.0). No potential was applied at the controls.

The *sampling* mode was also used in other experiments, where the spectrophotometric cuvette was filled with colloidal gold suspension during the measurement. Figures IV.6 and IV.7 show the absorbance at 523nm *vs.* electrodeposition time for 5 and 20nm colloidal gold particles. The absorbance change is higher for 20nm colloidal gold than for 5nm colloidal gold, although absolute absorbance values are higher for the 5nm colloidal gold electrodeposition, probably due to the

higher colloidal particle concentration in the spectrophotometric cuvette. Both plots show that short electrodeposition times (less than 5min) are preferable.

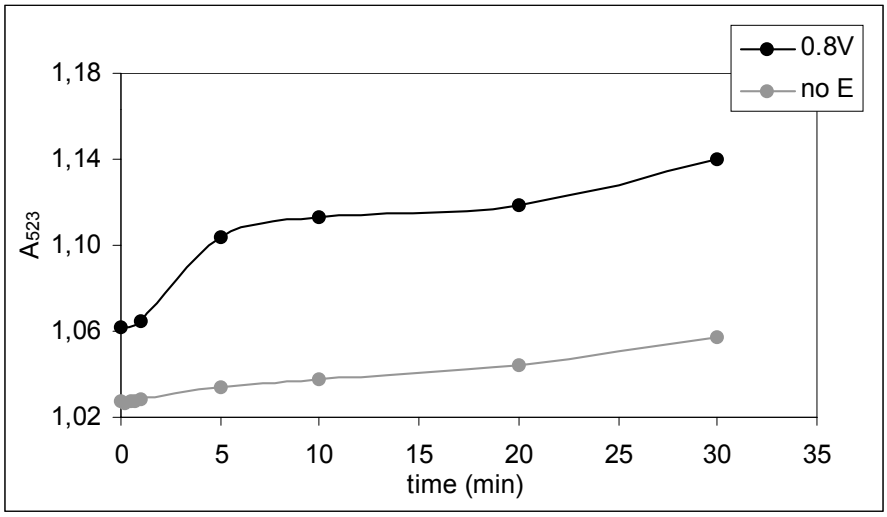

Figure IV.6. Absorbance at 523nm *vs.* time of 5nm colloidal gold electrodeposited or adsorbed on ITO electrodes in *sampling* mode. Electrodeposition conditions: application of +0.8V (*vs.* Ag/AgCl) for different times to a working ITO electrode immersed in a three-electrode cell containing 5nm colloidal gold suspension (4.4×10^{13} particles mL^{-1} in 10mM phosphate buffer, 0.1M NaCl, pH 7.0). No potential was applied at the controls.

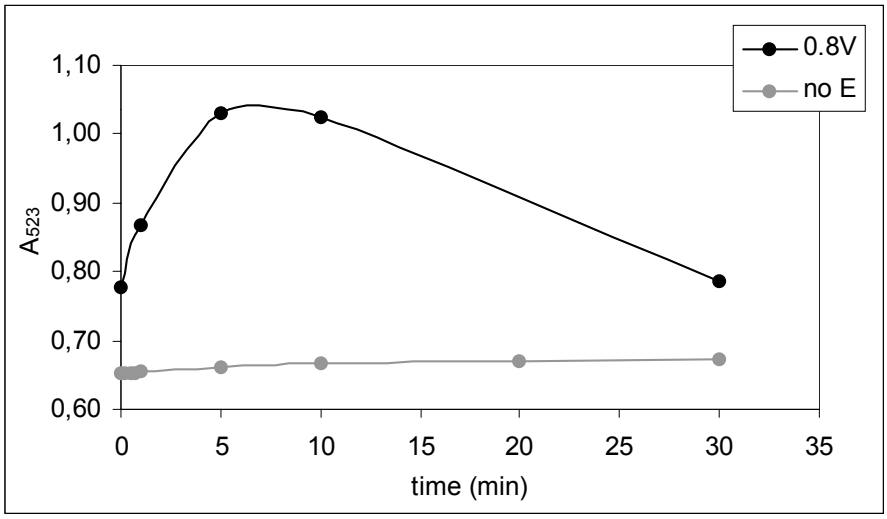

Figure IV.7. Absorbance at 523nm *vs.* time of 20nm colloidal gold electrodeposited or adsorbed on ITO electrodes in *sampling* mode. Electrodeposition conditions: application of +0.8V (*vs.* Ag/AgCl) for different times to a working ITO electrode immersed in a three-electrode cell containing 20nm colloidal gold suspension (5.2×10^{11} particles mL^{-1} in 10mM phosphate buffer, 0.1M NaCl, pH 7.0). No potential was applied at the controls.

The *real-time monitoring* mode provided similar results but higher reproducibility since the same area of the electrode was addressed continuously. Figure IV.8 shows the absorbance values for the electrodeposition of 5nm colloidal gold. It is possible to observe a different slope depending on if potential was applied or not, the slope of the electrodeposition being higher. No non-specific adsorption could be appreciated spectrophotometrically. Although in this case the measurement is

taken in a thin spectroelectrochemical cell, the difference in absorbance can still be appreciated probably due to the increased back scattering of the now immobilised particles.

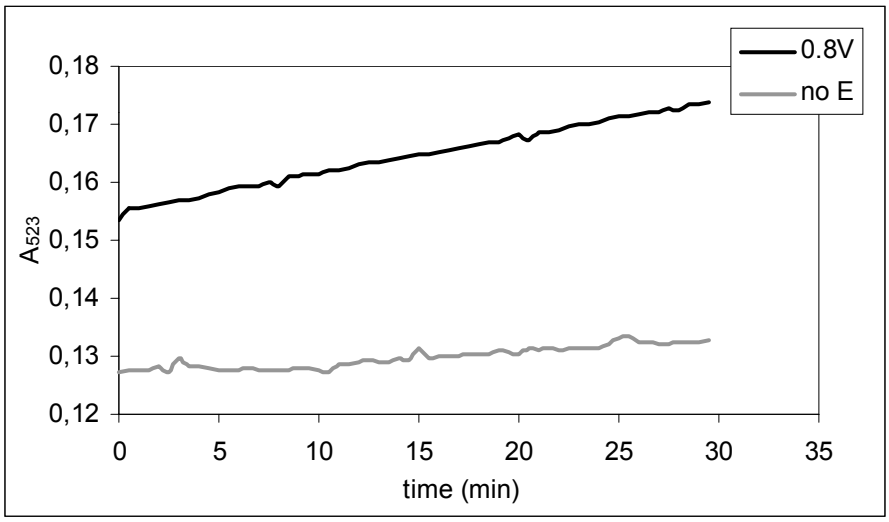

Figure IV.8. Absorbance at 523nm *vs.* time of 5nm colloidal gold electrodeposited or adsorbed on ITO electrodes in *real-time monitoring* mode. Electrodeposition conditions: application of +0.8V (*vs.* Ag/AgCl) in continuous to a working ITO electrode immersed in a three-electrode spectrophotoelectrochemical thin cuvette/cell containing 5nm colloidal gold suspension (4.4 x 10^{13} particles mL^{-1} in 10mM phosphate buffer, 0.1M NaCl, pH 7.0). No potential was applied at the controls.

It is interesting to note that in all the experiments with ITO, the first absorbance value for the electrodeposition was always higher than the corresponding non-specific adsorption one. This observation suggests that the highest electrodeposition rates may be occurring at times shorter than the time necessary to start the spectrophotometric measurement on this material.

Piezoelectric measurements with the electrochemical quartz crystal microbalance were also performed to study the colloidal gold electrodeposition. After injection of the colloidal gold suspension, there was a shift in frequency of 60Hz in 10min when applying +1.2V (*vs.* Ag/AgCl), while there was a flat line when potential was not applied (Figure IV.9). Our calculations, applying the Sauerbrey equation (1959), indicate that when a monolayer of colloidal gold particles is deposited on the electrode surface, the expected shift in frequency should be between 1140 and 1450Hz, depending on the packing density agreeing with other experimental results reported in the literature. Consequently, according to the observed shift in frequency, the electrodeposited colloidal gold particles correspond to approximately 5% of a monolayer. Although this result is difficult to explain and the experimental set up has to be optimised in order to make sure the observation is not an artefact, it indicates again that the application of potential selectively directs the electrodeposition of colloidal particles, whilst its absence leads to very little (if at all) non-specific adsorption.

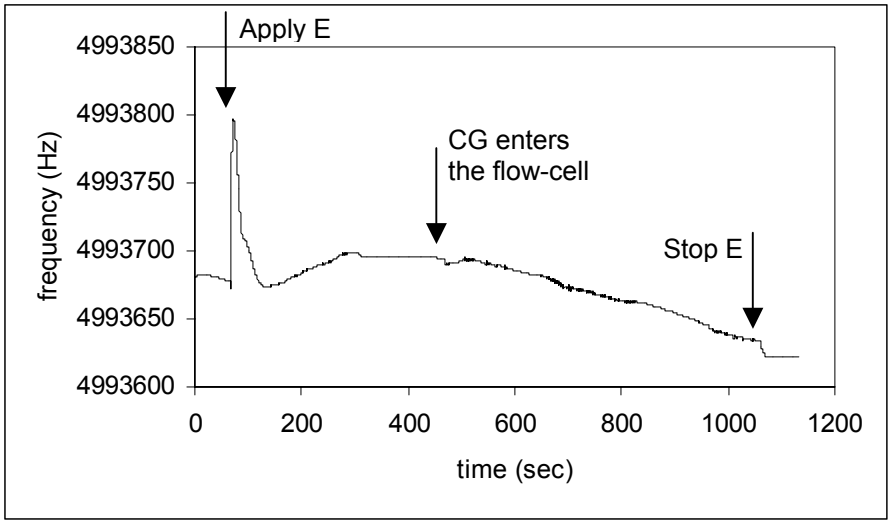

Figure IV.9. Frequency *vs.* time for the electrodeposition of 20nm colloidal gold on gold-covered quartz crystals. Experiment conditions: injection of 10mM tris-HCl buffer, 10mM KCl, 1% BSA, pH 7.0, at 75µL min^{-1}, application of +1.2V (*vs.* Ag/AgCl), and injection of the colloidal gold suspension (4.2 x 10^{11} particles mL^{-1} in the same buffer).

Removal of non-specifically adsorbed colloidal gold particles. It is necessary to mention that the experiments reported so far were performed under quiescent conditions (except the electrodeposition on gold-covered quartz crystals). However, the effect of shear stresses on the stability of colloidal gold suspensions is well known and quantified (Russel *et al.*, 1986). It is also of interest that Burdick *et al.* (2001) have shown that deposition is also a function of the Reynolds number of the mobile phase in contact with the electrode, especially when the roughness of the electrode surface is comparable or smaller than the particle characteristic dimension. Preliminary experiments were performed to observe if after the electrodeposition, non-specifically adsorbed particles could be removed if the electrodes were exposed to a flowing buffer solution at different Re. After the slow flow (Re = 1.85) the amount of electrodeposited material did not change significantly but unexpectedly, there was a 17-fold increase in the amount of non-specifically adsorbed material. In fact, the light microscopy images seem to show aggregation of the non-specifically adsorbed particles, which may interfere the phase analysis and give an artefact associated with the mobility that some authors have observed when particles deposit on surfaces (Trau *et al.*, 1996 and 1997). However, after the fast flow (Re = 164.48), whilst the amount of electrodeposited material decreased only by 25%, the amount of non-specifically adsorbed material decreased by 53% compared with the amount before any flow or 73% compared with the amount after the slow flow. Although experimental set-up and results analysis have to be optimised, these first observations are indicative of the possibility to remove non-specifically adsorbed particles by using flows with the appropriate Re values, or making the deposition under controlled hydrodynamic conditions.

HRP-bionanomodule arraying. Figure IV.10 shows the absorbance values from the colourimetric response of commercial TMB liquid substrate after electrodeposition or non-specific adsorption of HRP-colloidal gold on these electrodes. Absorbance values are higher when using 5min instead of 1min, due to the higher electrodeposition or non-specific adsorption of HRP-colloidal gold. However, whereas with 5min the absorbance value from the non-specific adsorption is 69% the value from the electrodeposited material, with 1min this non-specific adsorption is reduced to 58%. As noticed with free colloidal gold and spectrophotometry, at short times the difference between electrodeposition and non-specific or passive adsorption is higher. With this experiment it has been demonstrated that the electrodeposition of biorecognition nanomodules, in this case with HRP as a "proof of concept", is feasible.

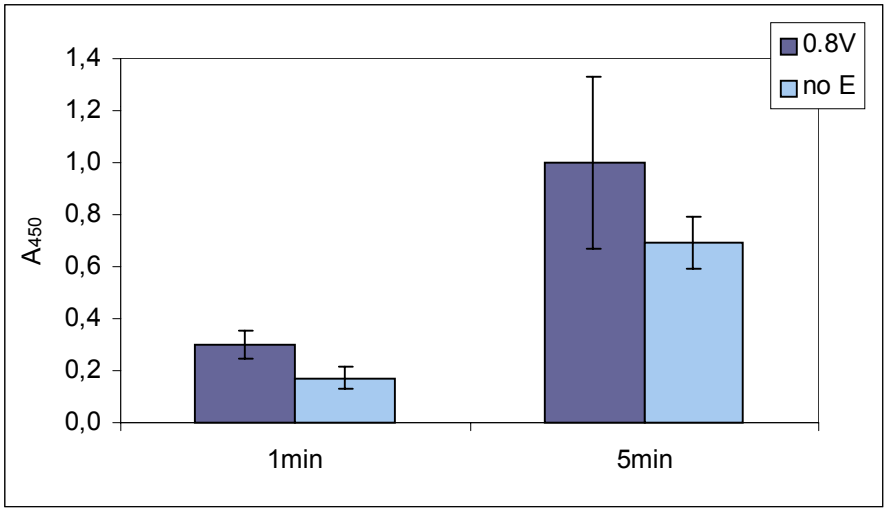

Figure IV.10. Absorbance at 450nm from the colourimetric reaction of the electrodeposited or adsorbed HRP-colloidal gold (10nm) with TMB on carbon screen-printed electrodes. Electrodeposition conditions: application of a 2-µL drop of HRP-colloidal gold conjugate suspension (3.2×10^{13} particles mL^{-1} in 50% glycerol with 0.15M NaCl, 0.01% MES, pH 6.5, 0.25% BSA) on the screen-printed electrodes, followed by application of +0.8V (*vs.* Ag/AgCl) for 1 and 5min. No potential was applied at the controls. Detection conditions: incubation of the modified electrodes in commercial TMB liquid substrate for 1h at 37°C with stirring, stopping of the reaction with H_2SO_4, and monitoring of the absorbance at 450nm.

Biorecognition nanomodule electrodeposition. The experiments described with colloidal gold suspensions with FITC-oligonucleotide-thiol-colloidal gold biorecognition nanomodules were repeated but in this case with electrodeposited conjugates. The FITC-oligonucleotide-thiol-colloidal gold conjugates were successfully deposited on the set of the IDEs at which potential had been applied (*results not shown*), showing the same appearance as the electrodeposition of bare colloidal gold. However, more extreme conditions (+1.6V (*vs.* Ag/AgCl) for 2h) had to be used in the electrodeposition, since milder conditions (+1.0V (*vs.* Ag/AgCl) for 30min) resulted in deposited material that was not detectable by microscopy. The electrodeposition was more difficult probably due to the coating of colloidal gold with biomolecules, which decreased the ability of the gold particles to be attracted by the potential wall or attached to gold. The FITC-oligonucleotide-thiol-colloidal gold-modified IDE was observed under fluorescence microscopy. However, the deposited

oligonucleotide did not emit any fluorescent signal. This quenching effect was probably due to the fluorescence resonance energy transfer (FRET) between FITC and gold.

The FITC-oligonucleotide-thiol-colloidal gold deposition on glassy carbon electrodes was detected electrochemically. Electrodes at which +1.1V (*vs.* Ag/AgCl) had been applied for 2min showed an oxidation peak at +1.6V (*vs.* Ag/AgCl), corresponding to the gold oxides formation, and a reduction peak at +1.3V (*vs.* Ag/AgCl), which might correspond to their reduction (Figure IV.11). The electrode at which no potential had been applied also showed lower oxidation and reduction peaks. Comparing the surface coverage, these peaks represented 26% of the specific electrodeposition. Lower potentials for higher times, +0.8V (*vs.* Ag/AgCl) for 5min and +0.6V (*vs.* Ag/AgCl) for 10min, resulted in higher non-specific adsorption ratios.

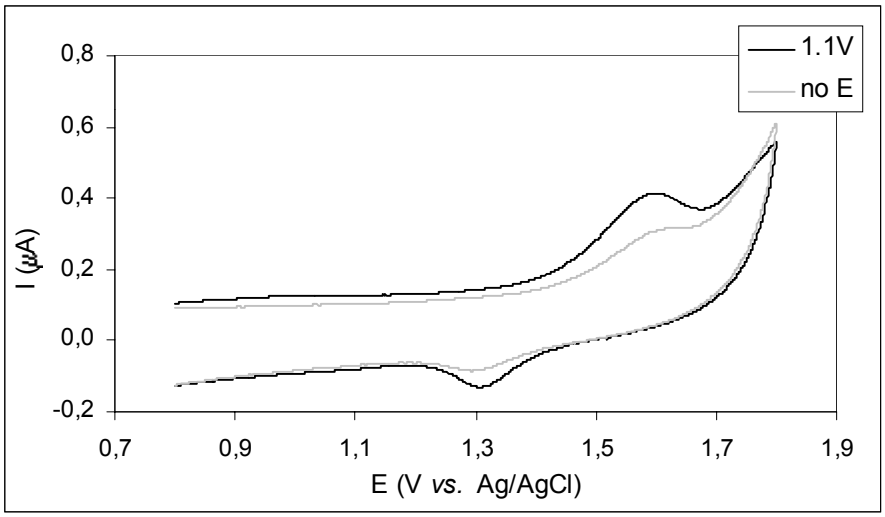

Figure IV.11. Cyclic voltammetry at 0.05mV s^{-1} in 0.1M H_2SO_4 of 1.5mm diameter glassy carbon electrodes after immersion of the electrode in a three-electrode cell containing a FITC-oligonucleotide-thiol-colloidal gold (20nm) conjugate suspension (7.7 x 10^{11} particles mL^{-1} in 10mM phosphate buffer, 0.1M NaCl, pH 7.0) and application of +1.1V (*vs.* Ag/AgCl) for 2min (dark blue). No potential was applied at the controls (light blue).

Sandwich ELONA was used on carbon screen-printed electrodes to verify the technique has the detection limit necessary to observe the electrodeposited biorecognition nanomodules and to verify the functionality of the same (Scheme IV.1). Figure IV.12 shows the results for this experiment. Although absorbance values were quite low and the background (blank) signal high, the total system with dig-oligonucleotide-thiol-colloidal gold gave higher response than the blanks without one of the steps or with FITC-oligonucleotide-thiol-colloidal gold conjugate, indicating that the sandwich can be built on the carbon screen-printed electrodes and detected colourimetrically. The results show that non-specific adsorption of the dig-oligonucleotide-thiol-colloidal gold conjugate on the screen-printed electrode surface (“no coating” bar) could not be appreciated, probably due to the presence of 1% BSA in the dig-oligonucleotide-thiol-colloidal gold conjugate suspension and on the electrode surface. BSA in the conjugate suspension blocks any possible remaining free sites of the dig-oligonucleotide-thiol-colloidal gold, inhibiting the subsequent adsorption on the BSA-coated

electrode. Moreover, there is not non-specific adsorption from the antidig-HRP label on any of the components of the system. Experiments with FITC-oligonucleotide-thiol-colloidal gold did not give any response, as expected since the conjugate does not have digoxigenin.

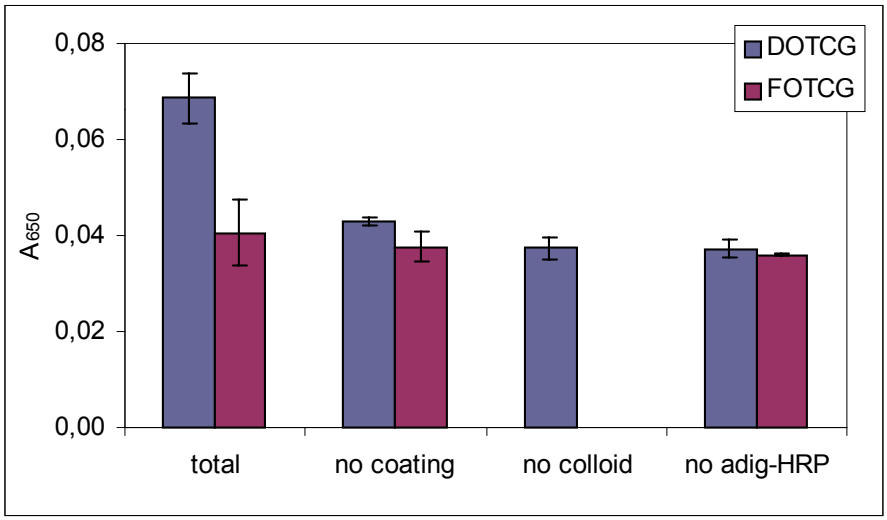

Figure IV.12. Absorbance at 650nm from the colourimetric reaction of the antidig-HRP with TMB in the sandwich ELONA on carbon screen-printed electrodes. Total: system as depicted in Scheme IV.1 with dig-oligonucleotide-thiol-colloidal gold (DOTCG) (20nm) (2.5 x 10^{10} particles mL^{-1} in 0.1M tris-HCl buffer, 0.1M KCl, pH 8.0, 1% BSA); no coating: blank without antidigoxigenin on the surface; no colloid: blank without conjugate; no adig-HRP: blank without antidig-HRP. FITC-oligonucleotide-thiol-colloidal gold (FOTCG) (20nm) conjugate suspension (2.3 x 10^{10} particles mL^{-1} in 0.1M tris-HCl buffer, 0.1M KCl, pH 8.0, 1% BSA) was used as a control. Detection conditions: incubation of the modified electrodes in commercial TMB liquid substrate for 1h at 37°C with stirring and monitoring of the absorbance at 650nm.

As can be seen in Figure IV.13, the electrodeposition experiment with colourimetric detection proved the selective deposition of the dig-oligonucleotide-thiol-colloidal gold conjugate on carbon screen-printed electrodes. Whilst the electrodes were only passive adsorption of the dig-oligonucleotide-thiol-colloidal gold conjugate show absorbance values not different from the blanks (with FITC-oligonucleotide-thiol-colloidal gold conjugate, without colloid or without antidig-HRP), the ones exposed to electrodeposition of the conjugate are almost three-fold higher, although the reproducibility achieved was low. The dig-oligonucleotide-thiol-colloidal gold conjugate did not adsorb non-specifically neither on the BSA-coated carbon electrode surface, probably due to the presence of 1% BSA in the dig-oligonucleotide-thiol-colloidal gold conjugate solution, nor on the non-coated carbon electrode surface. Moreover, the BSA coating of the electrode surface did not inhibit the electrodeposition, the same results as in the non-coated electrodes being obtained.

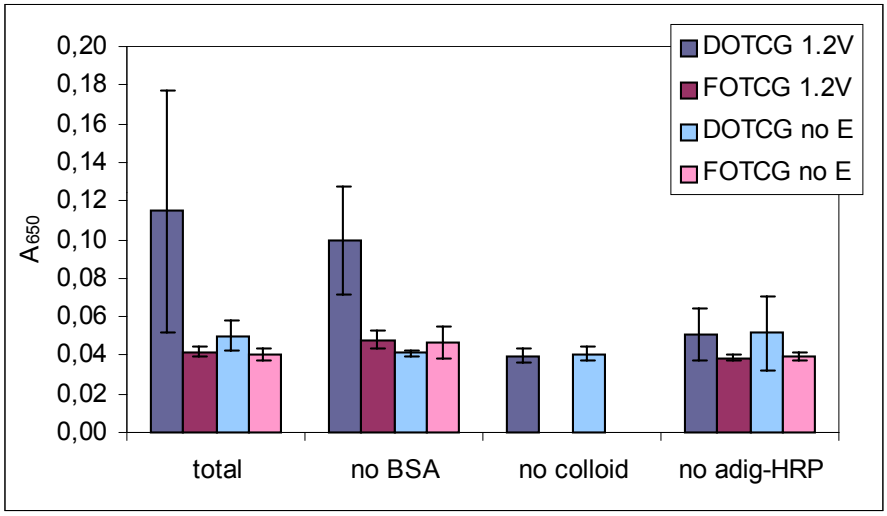

Figure IV.13. Absorbance at 650nm from the colourimetric reaction of the antidig-HRP with TMB due to the electrodeposited or adsorbed dig-oligonucleotide-thiol-colloidal gold (DOTCG) (20nm) on carbon screen-printed electrodes. Total: system as depicted in Scheme IV.2; no BSA: blank without the blocking step with BSA; no colloid: blank without conjugate; no adig-HRP: blank without antidig-HRP. Electrodeposition conditions: immersion of the carbon screen-printed electrode in a three-electrode cell containing a dig-oligonucleotide-thiol-colloidal gold (20nm) conjugate suspension (1.3 x 10^{12} particles mL^{-1} in 0.1M tris-HCl buffer, 0.1M KCl, pH 8.0, 1% BSA) and application of +1.2V (*vs.* Ag/AgCl) for 2min. No potential was applied at the controls. FITC-oligonucleotide-thiol-colloidal gold (FOTCG) (20nm) conjugate suspension (1.2 x 10^{12} particles mL^{-1} in 0.1M tris-HCl buffer, 0.1M KCl, pH 8.0, 1% BSA) was also used as a control. Detection conditions: incubation of the modified electrodes in commercial TMB liquid substrate for 1h at 37°C with stirring and monitoring of the absorbance at 650nm.

Figure IV.14 shows the background-subtracted electrochemical results with dig-oligonucleotide-thiol-colloidal gold conjugate for different measurement times to see if there is an optimal reading time with the highest signal/background ratio. Although electrodeposition intensity values are very low (20-24nA), it is possible to see that non-specific adsorption values are considerably lower. Whereas the electrodeposition currents are independent on the reading time, the non-specific adsorption intensity values show an increasing trend, the percentage compared to the electrodeposition being 14, 18, 20, 26 and 31% for 10, 15, 20, 30 and 60sec, suggesting that shorter times are the optimal reading conditions. This increase is related to the amplification due to the enzymatic reaction of the label. This 14% non-specific adsorption value demonstrates the viability of the strategy as arraying method and the use of amperometric detection. It is important to note that the non-specific adsorption is as important as the detection method used allows it to be. In this work, the detection method was not optimised and in fact, it can be appreciated from the high values of blanks (around 5nA) that it barely allows the detection of the electrodeposited nanomodules.

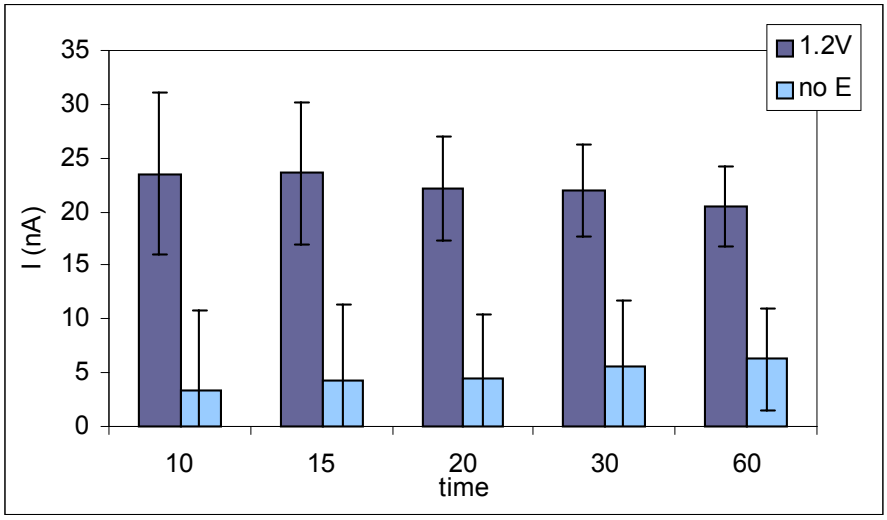

Figure IV.14. Currents obtained from the enzymatic reaction of the antidig-HRP with osmium complex due to the electrodeposited or adsorbed dig-oligonucleotide-thiol-colloidal gold (20nm) on carbon screen-printed electrodes. Intensity values are background-subtracted. Electrodeposition conditions: immersion of the carbon screen-printed electrode in a three-electrode cell containing a dig-oligonucleotide-thiol-colloidal gold (20nm) conjugate suspension (1.3 x 10^{12} particles mL^{-1} in 0.1M tris-HCl buffer, 0.1M KCl, pH 8.0, 1% BSA) and application of +1.2V (*vs.* Ag/AgCl) for 2min. No potential was applied at the controls. Detection conditions: incubation of 1µL of H_2O_2 (1:500 dilution in 50mM acetate buffer, 0.15M NaCl, pH 5.1) and 1µL of [Os(2,2'-bipyridine)$_2$Cl(4-(aminomethyl)pyridine)]Cl (0.2mM in water) on the working electrode for 2min, application of -0.1V (*vs.* Ag/AgCl) for 1min, and measuring of the current values at different times.

The dig-oligonucleotide-thiol-colloidal gold conjugate was also electrodeposited on photolithographed gold 3-electrode arrays. The two gold electrodes where the drop was placed were 1mm in diameter and the distance between them was 2mm. Due to evaporation effects, short deposition times (to 10min) were used. Figure IV.15 shows the light microscopy images for the blank electrodes whre no sample (a) or potential (b) were applied and the working electrode at which +0.8V (*vs.* Ag/AgCl) was applied for 10min (c).

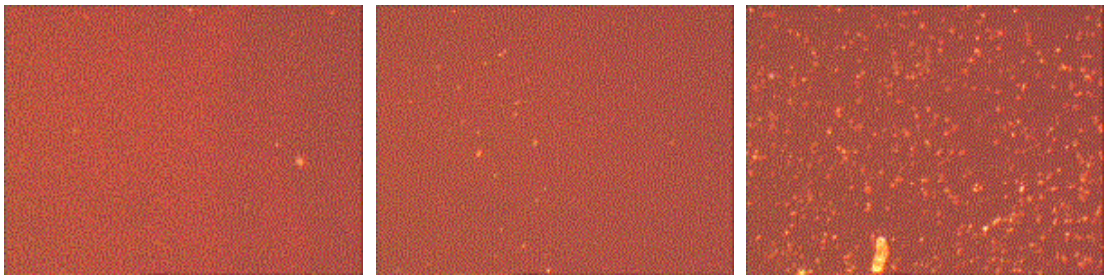

Figure IV.15. Light microscopy images of the electrodeposition of dig-oligonucleotide-thiol-colloidal gold (3nm) on photolithographed gold 3-electrode arrays. a) Bare gold electrode; b) gold electrode after incubation with dig-oligonucleotide-thiol-colloidal gold for 10min; c) gold electrode after electrodeposition with dig-oligonucleotide-thiol-colloidal gold for 10min at +0.8V (*vs.* Ag/AgCl).

The light dots, much more abundant when applying potential, demonstrate that the dig-oligonucleotide-thiol-colloidal gold conjugate was electrodeposited to a much higher extent than non-specifically adsorbed. Using the phase analysis of the microscope AnalySIS software, the

percentage of the area covered by colloidal gold was approximately 0.05, 0.30 and 3.99% for the bare electrode, the electrode where no potential was applied and the electrode where +0.8V (*vs.* Ag/AgCl) was applied for 10min, respectively. These values show that the non-specific adsorption is 7.5% of the specific deposition. It should be noted that these observations also give an indication of some nucleation phenomena upon deposition (the observed dots are approximately 20μm in diameter), probably on surface imperfections.

In Figure IV.16, +1.6V (*vs.* Ag/AgCl) was applied to the working electrode for 10min. In this case, the number of light dots increases, suggesting that there is more electrodeposited material. However, the deposition is less homogeneous, and the presence of aggregates is noticeable. Using the phase analysis, the percentage of the area covered by colloidal gold is approximately 0.05, 1.81 and 53.21% for the bare electrode, the electrode where no potential was applied and the electrode where +1.6V (*vs.* Ag/AgCl) was applied for 10min, respectively. In this case, the non-specific adsorption is 3.4% of the specific deposition. At higher potentials (+1.9V (*vs.* Ag/AgCl)), depositions were more evident and moreover and they could be achieved at shorter times (1min), but they lacked homogeneity. Despite the experimental error in the percentages (as evidenced by the difference between the 0.30 and the 1.81% obtained for the electrodes where no potential was applied in Figures IV.15 and IV.16), the values demonstrate the successful directed electrodeposition of the biorecognition nanomodules. It was decided that for this system, the optimum dig-oligonucleotide-thiol-colloidal gold conjugate electrodeposition conditions are +0.8V (*vs.* Ag/AgCl) for 10min.

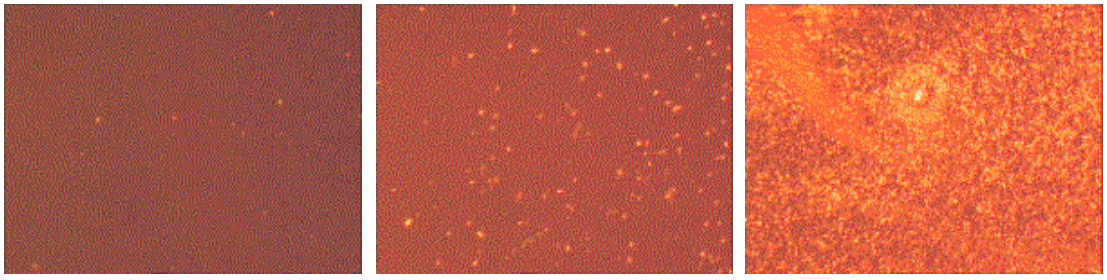

Figure IV.16. Light microscopy images of the electrodeposition of dig-oligonucleotide-thiol colloidal gold (3nm) on photolithographed gold 3-electrode arrays a) Bare gold electrode; b) gold electrode after incubation with dig-oligonucleotide-thiol-colloidal gold for 10min; c) gold electrode after electrodeposition with dig-oligonucleotide-thiol-colloidal gold for 10min at +1.6V (*vs.* Ag/AgCl).

Functionality of electroarrayed biorecognition nanomodules. The *hybridisation* ELONA with the dig-oligonucleotide-thiol-colloidal gold conjugate was performed also on carbon screen-printed electrodes. Although the *hybridisation* ELONA was successful in plate wells (*see Chapter III*), in the case of spectrophotometric detection of hybridisation on the surface of carbon screen-printed electrodes, there was little difference between signal and background. Control experiments indicated that there was a high non-specific adsorption of streptavidin-HRP either on the electrode

surface or on the polycarbonate substrate on which the electrodes were screen-printed. Several experiments demonstrated that high non-specific adsorption of streptavidin-HRP was produced on the polycarbonate substrate.

Although the colourimetric detection was not suitable, the electrochemical detection offered the possibility to detect the hybridisation event on screen-printed electrodes because in the electrochemical mode only the response from the working electrode (and not from the substrate surface) is measured. Figure IV.17 plots the background-subtracted electrochemical responses at 10sec for the electrodeposition and non-specific adsorption of the dig-oligonucleotide-thiol-colloidal gold conjugate followed by hybridisation with biotin-labelled complementary and oligonucleotides with 4-point mutations (background currents being around 5nA).

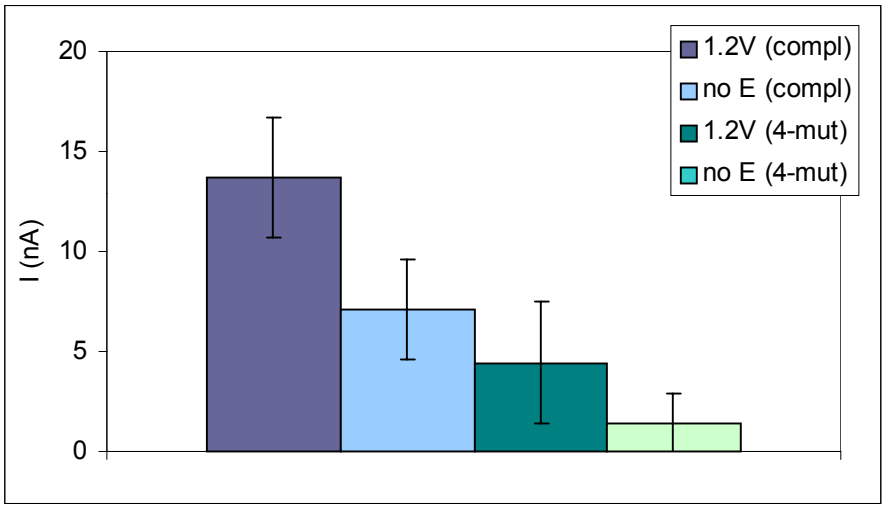

Figure IV.17. Currents obtained from the enzymatic reaction of the streptavidin-HRP with osmium complex due to the electrodeposited or adsorbed dig-oligonucleotide-thiol-colloidal gold (20nm) on carbon screen-printed electrodes and subsequent hybridisation. Intensity values are background-subtracted. Electrodeposition conditions: immersion of the carbon screen-printed electrode in a three-electrode cell containing a dig-oligonucleotide-thiol-colloidal gold (20nm) conjugate suspension (1.3 x 10^{12} particles mL^{-1} in 0.1M tris-HCl buffer, 0.1M KCl, pH 8.0, 1% BSA) and application of +1.2V (*vs.* Ag/AgCl) for 2min. No potential was applied at the controls. Hybridisation conditions: incubation with a solution of biotin-labelled complementary oligonucleotide, non-labelled complementary oligonucleotide or biotin-labelled oligonucleotide with 4 point mutations (5μg mL^{-1} in 10mM tris-HCl, 1mM EDTA, 0.3 x SSC, 2 x Denhardt's solution, pH 8.0) for 1h at 55°C. Detection conditions: incubation of 1μL of H_2O_2 (1:500 dilution in 50mM acetate buffer, 0.15M NaCl, pH 5.1) and 1μL of [Os(2,2'-bipyridine)$_2$Cl(4-(aminomethyl)pyridine)]Cl (0.2mM in water) on the working electrode for 2min, application of -0.1V (*vs.* Ag/AgCl) for 1min, and measuring of the current values at 10sec.

As expected, the current intensity values from hybridisation of electrodeposited biorecognition nanomodules with complementary sequences are the highest ones, the values from hybridisation of non-specifically adsorbed biorecognition modules with the same complementary sequences being 52%. The current from hybridisation of electrodeposited biorecognition nanomodules with mutated sequences is 32% (compared with the hybridisation with complementary sequences), and the current from hybridisation of non-specifically adsorbed biorecognition nanomodules with mutated sequences is also 32% (compared with the hybridisation with complementary sequences). It can be seen that there is selective electrodeposition of the dig-oligonucleotide-thiol-colloidal gold conjugate

on carbon screen-printed electrodes, this oligonucleotide-colloidal gold conjugate can be hybridised, and the response can be monitored electrochemically. Moreover, the electrochemical DNA sensor can differentiate 4-point mutations in a 19-mer oligonucleotide. Electrochemical amplification systems are being investigated in order to increase the current arising from the hybridisation detection, which will provide the possibility of further miniaturisation.

Conclusions

Oligonucleotide biorecognition nanomodules can be site selectively electrodeposited on IDEs, glassy carbon electrodes, gold 3-electrode arrays and carbon screen-printed electrodes, and the selective electrodeposition can be followed by light microscopy, colourimetry and electrochemical methods. Despite the clear differences between electrodeposition and non-specific adsorption, the later still gives a “stray” 14% signal in the electrochemical detection. Absorbance and currents were very low compared to blanks, suggesting the necessity for a signal amplification system. Preliminary experiments suggested that non-specifically adsorbed particles could be removed by using a flow system with an appropriate Re. Finally, electrodeposited biorecognition nanomodules were functional and able to differentiate 4 mutations in a 19-mer oligonucleotide sequence, demonstrating that the strategy can be used in low-cost DNA sensor arrays. Again, electrochemical currents were very low, suggesting that signal amplification is required for efficient amperometric detection of hybridisation events.

References

Adamczyk Z., Siwek B., Zembala M., and Belouschek P., *Adv. Colloid. Interface Sci.*, **1994**, 48, 151.

Adamczyk Z., Siwek B., Zembala M., and Weroński P., *J. Colloid. Interface Sci.*, **1997**, 185, 236.

Adamczyk Z. and Weroński P., *J. Colloid. Interface Sci.*, **1997**, 189, 348.

Bailey R.C., Stevenson K.J., and Hupp J.T., *Adv. Mater.*, **2000**, 12 (24), 1930.

Burdick G.M., Berman N.S., and Beaudoin S.P., *J. Nanoparticle Res.*, **2001**, 3, 455.

Castellino A.M., *Genome Res.*, **1997**, 7, 943.

Crumbliss A.L., Perine S.C., Stonehuerner J., Tubergen K.R., Zhao J., Henkens R.W., and O’Daly J.P., *Biotechnol. Bioeng.*, **1992**, 40 (4), 483.

Despić A.R. and Pavlović M.G., *J. Electroanal. Chem.*, **1984**, 180, 31.

Drobyshev A., Mologina N., Shik V., Pobedimskaya D., Yershov G., and Mirzabekov A., *Gene*, **1997**, 188, 45.

Faraudo J. and Bafaluy J., *Europhys. Lett.*, **1999**, 46 (4), 505.

Fodor S.P.A., Read J.L., Pirrung M.C., Stryer L., Lu A.T., and Solas D., *Science*, **1991**, 251, 767.

Giersig M. and Mulvaney P, *J. Phys. Chem.*, **1993**, 97, 6334.

Grabar K.C., Smith P.C., Musick M.D., Davis J.A., Walter D.G., Jackson M.A., Guthrie A.P., and Natan M.J., *J. Am. Chem. Soc.*, **1996**, 118 (5), 1148.

Guschin D., Yershov G., Zaslavsky A., Gemmell A., Shick V., Proudnikov D., Arenkov P., and Mirzabekov A., *Anal. Biochem.*, **1997**, 250, 203.

Lavalle P., Schaaf P., Ostafin M., Voegel J.-C., and Senger B., *Prot. Natl. Acad. Sci. USA*, **1999**, 96, 11100.

Livache T., Roget A., Dejean E., Barthet C., Bidan G., and Téoule R., *Nucleic Acids Res.*, **1994**, 22 (15), 2915.

Livache T., Roget A., Dejean E., Barthet C., Bidan G., and Téoule R., *Synthetic Metals*, **1995**, 71, 2143.

Livache T., Fouque B., Roget A., Marchand J., Bidan G., Téoule R., and Mathis G., *Anal. Biochem.*, **1998**, 255, 188.

Pease A.C., Solas D., Sullivan E.J., Cronin M.T., Holmes C.P., and Fodor S.P.A., *Proc. Natl. Acad. Sci.*, **1994**, 91, 5022.

Roget A., Livache T., Marchand J., and Téoule R., *Nucleosides Nucleotides*, **1995**, 14 (3-5), 943.

Russel W.B., Saville D.A., and Schowalter W.R., *Colloidal dispersions*, Cambridge University Press, Cambridge, United Kingdom, **1989**.

Sakai K., Higuchi H., Matsubara K., and Kato K., *Anal. Biochem.*, **2000**, 287, 32.

Sato T. and Ahmed H., *Appl. Phys. Lett.*, **1997**, 70 (20), 2759.

Sauerbrey G.Z., *Z. Phys.*, **1959**, 155, 206.

Trau M., Saville D.A., and Aksay I.A., *Science*, **1996**, 272, 706.

Trau M., Saville D.A., and Aksay I.A., *Langmuir*, **1997**, 13 (24), 6375.

Wojtaszczyk P., Bonet Ávalos J., and Rubí J.M., *Europhys. Lett.*, **1997**, 40 (3), 299.

Yershov G., Barsky V., Belgovskiy A., Kirillov E., Kreindlin E., Ivanov I., Parinov S., Guschin D., Drobishev A., Dubiley S., and Mirzabekov A., *Proc. Natl. Acad. Sci.*, **1996**, 93, 4913.

Zammatteo N., Jeanmart L., Hamels S., Courtois S., Louette P., Hevesi L., and Remacle J., *Anal. Biochem.*, **2000**, 280, 143.

Abbreviations

BSA: bovine serum albumin

CCD: charge-coupled device

CV: cyclic voltammetry

dig: digoxigenin

DNA: deoxyribonucleic acid

DOTCG: digoxigenin-oligonucleotide-thiol colloidal gold

ELONA: enzyme-linked oligonucleotide assay

FITC: fluorescein-isothiocyanate

FOTCG: FITC-oligonucleotide-thiol colloidal gold

GOx. glucose oxidase

HRP: horseradish peroxidase

IDEs: interdigitated electrodes

ITO: indium-tin oxide

LSV: linear sweep voltammetry

MES: 2-morpholinoethanesulfonic acid

TMB: 3,3',5,5'-tetramethyl-benzidine

tris-HCl: tris[hydroxymethyl]aminomethane hydrochloride

Tween 20: polyoxyethylenesorbitan monolaurate